Rare-earth spin-glasses with uniaxial anisotropy

K. Baberschke,* P. Pureur, and A. Fert
Laboratoire de Physique des Solides associé au Centre Nationale de la Recherche Scientifique, Université de Paris-Sud, 91405 Orsay Cedex, France

R. Wendler
Institut für Atom- und Festkörperphysik, Freie Universität Berlin, Arnimallee 14, D-1000 Berlin 33, West Germany

S. Senoussi
Laboratoire de Physique des Solides associé au Centre Nationale de la Recherche Scientifique, Université de Paris-Sud, 91405 Orsay Cedex, France
(Received 19 December 1983)

The properties of spin-glasses with uniaxial anisotropy are investigated by magnetization measurements on single crystals of Y and Sc doped with Er, Dy, Tb, or Gd impurities. In alloys with strong anisotropy, spin-glass properties (susceptibility, cusp, irreversibility) appear only for fields along the c axis of the crystal (Ising-like systems) or only for fields in the basal plane (X-Y—like systems). The freezing temperature of the Ising-like systems is higher than that of the Heisenberg systems (alloys with Gd) by about a factor of 3. These results are in agreement with recent theoretical predictions. In alloys with small anisotropy, the irreversibility effects appear at the same temperature in longitudinal and transverse fields and we cannot identify the two-stage freezing predicted by the theory.

I. INTRODUCTION

The properties of metallic spin-glasses (SG) with uniaxial single-ion anisotropy are beginning to be extensively studied.[1–6] The starting point of most of the theoretical approaches[1,2] is an extension of the Sherrington-Kirkpatrick (SK) Hamiltonian:[7]

$$\mathscr{H}=-\sum_{ij}J_{ij}\vec{S}_i\cdot\vec{S}_j-D\sum_i S_{iz}^2-g\mu_B\vec{H}\cdot\sum_i\vec{S}_i\ . \tag{1}$$

The first term describes the interaction of classical vectors coupled via a set of infinite-range exchanges $\{J_{ij}\}$ whose probability distribution is

$$P(J_{ij})=\left[\frac{N}{2\pi j^2}\right]^{1/2}\exp[-N(J_{ij}/N)^2/2j^2]\ . \tag{2}$$

The second term of Eq. (1) accounts for a uniaxial crystal field and the third term for the interaction with an applied field. We show in Fig. 1 the phase diagram predicted by Roberts and Bray[2] and Cragg and Sherrington.[1]

For $D>0$ and $D/j\gg1$ the Hamiltonian $\mathscr{H}$, Eq. (1), is equivalent to an Ising-type SK Hamiltonian. This is consistent with the top of the phase diagram, Fig. 1, showing a freezing of the longitudinal spin components at $T/j=3$.

For $D<0$ and $|D|/j\gg1$, the Hamiltonian $\mathscr{H}$ is equivalent to an X-Y—type SK Hamiltonian. This is again consistent with the lowest part of the phase diagram, Fig. 1, showing a freezing of the transverse components at $T/j=1.5$.

For $D=0$, the Hamiltonian is a Heisenberg-type SK Hamiltonian, which is consistent with a freezing of both the longitudinal and transverse components at $T/j=1$.

The difference between the values of T_g/j in the Ising, X-Y, and Heisenberg limits (3, 1.5, and 1, respectively) is a remarkable feature of the mean-field model of spin-glasses.[7,8] Such a difference has never been confirmed by experiments because it is generally very difficult to know the relative values of j in different systems. In this

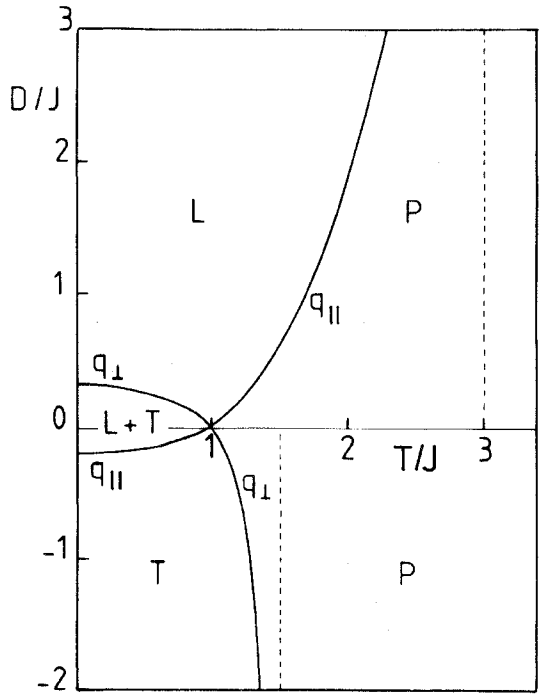

FIG. 1. Schematic phase diagram for a spin-glass with infinite-range interactions and uniaxial anisotropy. For notation see Eqs. (1) and (2) and Refs. 1 and 2.

respect, the $Y\mathscr{R}$ and $Sc\mathscr{R}$ (where $\mathscr{R}$ represents a rare-earth element) alloys present two advantages: First, there exist Ising-, X-Y—, and Heisenberg-like ions and second, the ratio between the values of j for two different rare earths (RE) in the same host is known. One of the motivations of this work was to study the spin-glass properties in the Ising, X-Y, and Heisenberg limits and to probe the theoretical predictions for the relative values of T_g/j.

For intermediate values of D/j the models of Refs. 1 and 2 describe the progressive change from an Ising or X-Y spin-glass to a Heisenberg spin-glass. At sufficiently large values of $|D|/j$ they predict the freezing of only one spin component (longitudinal for $D>0$, transverse for $D<0$). At sufficiently small values of $|D|/j$ they predict the successive freezing of the two components at different temperatures; see the phases L and LT and T and LT in Fig. 1. How the crossing of the lower phase boundary should show up in magnetization experiments cannot be predicted. One could imagine that irreversibility effects will appear at different temperatures in transverse and longitudinal fields. Alternatively, one could also imagine that the irreversibility effects will appear for both directions at the upper phase boundary. To clarify this aspect of the problem was also a motivation of our work.

We report in this paper on magnetization measurements on single crystals of Y and Sc containing Er, Dy, Tb, and Gd impurities. The crystal-field parameters are well known.[9,10] YEr and ScEr are expected to be Ising-like systems ($D>0$), while the alloys with Dy and Tb are expected to be X-Y—like ($D<0$). The ratios D/j can be changed by varying the RE concentration, which allows us to go from the Ising or X-Y limit at low concentrations to intermediate situations at high concentrations. For YGd and ScGd, D is very small ($\sim 4\times 10^{-3}$ K). Their magnetic properties appear to be not exactly, but almost, isotropic. We shall present these properties and discuss the possible origin of their small anisotropy in a separate publication. In this paper we shall only report on their cusp temperature, which we shall take as characteristic of Heisenberg systems.

This work is similar to the experiments on Mn in Zn, Cd, and Mg by Albrecht *et al.*[3] An important difference is that we can compare the behavior of different ions in *one host* while, for example, a quantitative comparison of *Zn*Mn and *Cd*Mn is difficult.

The paper is organized in the following way. In Sec. II we adapt the vector spin Hamiltonian, Eq. (1), to our systems containing RE ions with quantum moments $\vec{J}$. We present our experimental results in Sec. III and a discussion of these results in Sec. IV. It will be shown that while some of the properties predicted by the theory are found in our experiment, other results are in conflict with the theory. Finally, we would like to stress that the appearance of cooperative magnetic properties in only one or two directions of the lattice structure is not surprising; it follows directly from the physics of single ions. A more important question is to see if the different behaviors observed for different directions are well described by the mean-field spin-glass model.

II. CRYSTAL-FIELD AND EXCHANGE INTERACTIONS FOR THE RE'S IN Y AND SC

The crystal-field (CF) Hamiltonian for RE ions in hexagonal symmetry is given by[11]

$$\mathscr{H}_{\mathrm{CF}}=B_2^0 O_2^0(\vec{J})+B_4^0 O_4^0(\vec{J})+B_6^0 O_6^0(\vec{J})+B_6^6 O_6^6(\vec{J}) \qquad (3)$$

with $O_2^0\equiv 3J_z^2-J(J+1)$.

We give in Table I the values of the crystal-field coefficients $B_2^0, B_4^0, B_6^0, B_6^6$ extracted from experiments on dilute Y- and Sc-based alloys.[9,10] $B_2^0 O_2^0$ is the largest term in Eq. (3) and determines the main features of the magnetic behavior, i.e., easy magnetization along the c axis for $B_{20}<0$ or easy magnetization in the basal plane for $B_{20}>0$. The other terms also influence the magnetic properties. For example, the term $B_6^6\ O_6^6$ can mix states $|J_z=M\rangle$ and $|J_z=M\pm 6\rangle$ and thereby changes somewhat the wave function of the ground state (see Table I). However, in general, the influence of the fourth- and sixth-order terms is not very significant. Since we want to compare our experimental results to the predictions of

TABLE I. Crystal-field parameters, overall crystal-field splitting, and wave function of the ground state for several rare-earth ions in Sc or Y (from Ref. 9). ξ_J is the de Gennes factor [$\xi_J=\frac{1}{3}J(J+1)(g_J-1)^2$]. In YTb and ScTb there are several states in a small-energy range (7 K in YTb, 8 K in ScTb) above the lowest level. We give the wave function of all these states.

Impurities (de Gennes factor)	Host	B_2^0 (K)	B_4^0 (10^{-3} K)	B_6^0 (10^{-5} K)	B_6^6 (10^{-4} K)	Δ/K	Ground state
Er	Y	−0.29	0.6	2.4	2.8	123	$0.97\,\lvert+\frac{13}{2}\rangle-0.23\,\lvert\pm\frac{1}{2}\rangle+0.12\,\lvert\pm\frac{11}{2}\rangle$
($\xi_J=2.55$)	Sc	−0.07	0.36	3.6	−2.6	156	$0.83\,\lvert\pm\frac{13}{2}\rangle-0.48\,\lvert\pm\frac{1}{2}\rangle+0.27\,\lvert\pm\frac{11}{2}\rangle$
Dy	Y	0.33	−2.8	3.8	−3.6	170	$0.22\,\lvert\pm\frac{13}{2}\rangle-0.95\,\lvert\pm\frac{1}{2}\rangle+0.20\,\lvert\mp\frac{11}{2}\rangle$
($\xi_J=7.08$)	Sc	0.19	−0.86	2.0	−2.1	90	$0.29\,\lvert\pm\frac{13}{2}\rangle-0.92\,\lvert\pm\frac{1}{2}\rangle+0.29\,\lvert\mp\frac{11}{2}\rangle$
Tb	Y	0.89	0.55	−1.32	1.0	90	$0.041\,\lvert\pm5\rangle+0.999\,\lvert\mp1\rangle$ $0.015\,\lvert\pm6\rangle+1.000\,\lvert0\rangle+0.015\,\lvert6,-6\rangle$ $0.115\,\lvert\pm4\rangle+0.993\,\lvert6,\mp2\rangle$
($\xi_J=10.5$)	Sc	0.31	−8.3	7.9	−7.6	53	$0.61\,\lvert\pm4\rangle+0.79\,\lvert\mp2\rangle$ $0.7\,\lvert3\rangle+0.7\,\lvert-3\rangle$

TABLE II. T_g, T_g/j, and D/j for our single crystal and polycrystal (p) alloys. T_g is the temperature of the splitting between ZFC and FC susceptibility curves in very small fields. T_g/j and D/j are calculated as described in Sec. II.

Alloy	Concentration (at. %)	T_g (K)	T_g/j	D/j
*Y*Er	2	1.93	2.71	28.4
	4	3.9	2.75	19.2
	5	5.6	3.16	11.3
*Sc*Er	10	3.4	3.07	4.07
	15 p	4.1	2.49	2.71
	20 p	5.4	2.46	2.03
*Y*Dy	3	9.2	3.11	−7.12
*Sc*Dy	5	4.7	3.12	−7.95
	9.5 p	8	2.76	−4.19
	14.6 p	11.4	2.57	−2.72
	19 p	16.4	2.83	−2.09
*Y*Tb	1	3.2	2.2	−25.6
	2 p	8.5		
*Sc*Tb	4.5	6.25	3.05	−6.41
*Y*Gd	1	2.1	1	~0
*Sc*Gd	5	3.5	1.02	~0
	15	10	1.08	~0

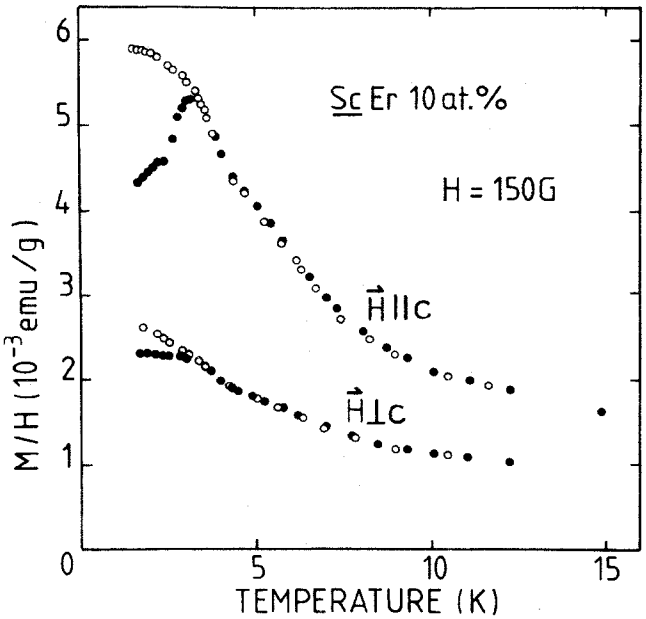

FIG. 2. ZFC (●) and FC (○) susceptibilities of *Sc*Er 10 at. % in longitudinal and transverse fields (150 G). The ZFC and FC curves split at the temperature of the cusp of $\chi_{\parallel}^{\mathrm{ZFC}}$.

models based on Eq. (1), which contains only quadratic CF terms, we neglect the fourth- and sixth-order terms.

Our total Hamiltonian, including the crystal-field, the exchange, and Zeeman interactions is written as

$$\mathcal{H}=-\sum_{ij}\Gamma_{ij}(g_J-1)^2\vec{J}_i\cdot\vec{J}_j+\sum_i B_2^0 J_{iz}^2-g_J\mu_B\vec{H}\cdot\sum_i\vec{J}_i\ . \tag{4}$$

We have included the de Gennes coefficient $(g_J-1)^2$ in the expression for the exchange term to explicitly show that the exchange coefficient for different RE ions in the same host scales as $(g_J-1)^2$. Equation (4) can be rewritten in the form of a classical spin Hamiltonian by replacing the quantum spin operators $\vec{J}$ with classical vectors of the same length:

$$\vec{J}\rightarrow\frac{\sqrt{J(J+1)}}{\sqrt{3}}\vec{S}\ , \tag{5}$$

where $\vec{S}$ is a vector of length $\sqrt{3}$. A vector spin Hamiltonian of the form of Eq. (1) is thus obtained with

$$J_{ij}=\frac{J(J+1)}{3}(g_J-1)^2\Gamma_{ij}\ , \tag{6}$$

$$D=-\frac{J(J+1)}{3}B_2^0\ . \tag{7}$$

Adopting the conventional assumption of a distribution width of the Γ_{ij} exchange coefficients proportional to the concentration c, the parameter j is written as

$$j=c\frac{J(J+1)}{3}(g_J-1)^2\Gamma=c\xi_J\Gamma\ , \tag{8}$$

where the coefficient $\xi_J=\frac{1}{3}J(J+1)(g_J-1)^2$ depends only on the RE element, while the coefficient Γ depends only on the host (Sc or Y). Finally, the ratios T/j and D/j involved in the phase diagram of Fig. 1 must be replaced by the following ratios:

$$T/j\rightarrow T/(c\xi_J\Gamma)\ , \tag{9}$$

$$D/j\rightarrow -B_2^0/[c(g_J-1)^2\Gamma]\ . \tag{10}$$

Γ is a common coefficient for all the RE's in a given host but is unknown. We shall adopt the value of Γ giving $T_g/j=1$ for the quasi-Heisenberg alloys containing *S*-state ions, i.e., *Sc*Gd and *Y*Gd. For *Sc*Gd, T_g is proportional to c, so that we can choose Γ_{Sc} so that $T_g/j=1$ for all the concentrations. For *Y*Gd, T_g is not exactly proportional to c and we have chosen Γ_{Y} so that $T_g/j=1$ for *Y*Gd 1 at. %. The values Γ_{Y} and Γ_{Sc} are in the ratio $\Gamma_{\mathrm{Y}}/\Gamma_{\mathrm{Sc}}=3.25$. We show in Table II the values of D/j calculated in the above mentioned way for all our alloys. D/j is positive for the alloys with Er and negative for the alloys with Dy and Tb. We see that $|D/j|$ is systematically smaller in the Sc-based alloys than in the Y-based alloys (larger values of $|D/j|$ in Sc-based alloys would imply smaller concentrations, lowering T_g and therefore measurements at lower temperatures).

III. EXPERIMENTAL RESULTS

We present magnetization measurements on a series of Sc- and Y-based single crystals containing Er, Dy, Tb, or Gd impurities. Most of the single crystals have been made by strain annealing. We measured their magnetization by using a Foner-type magnetometer.

A. *Sc*Er and *Y* Er (Ising-like alloys)

We show in Figs. 2 and 3 the field cooling (FC) and zero field cooling (ZFC) susceptibilities of *Sc*Er 10 at. %

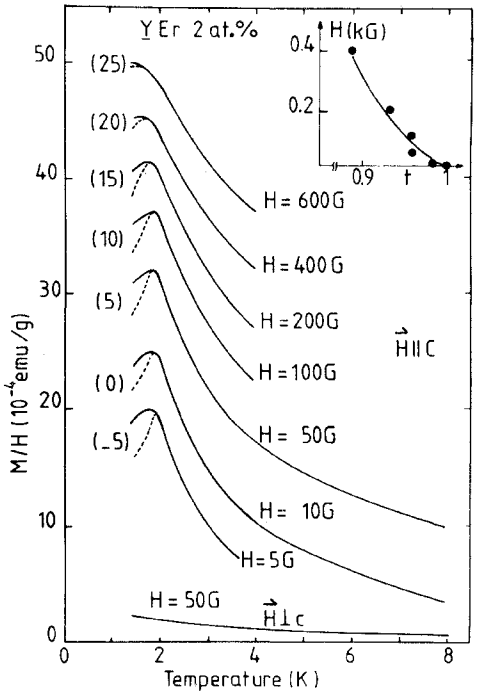

FIG. 3. ZFC (dashed line) and FC (solid line) susceptibilities of YEr 2 at. % in longitudinal and transverse fields. The longitudinal susceptibility is shown for several values of the field. The curve for 10 G corresponds to the scale of the vertical axis; the curves for other fields are shown with an offset of 5,10,.... Inset: Field H vs $T=\Theta/T_g$, where Θ is defined as the temperature of the splitting between the FC and ZFC susceptibility. The solid line corresponds to $H^{2/3}\sim 1-t$. $T_g=\Theta(H\to 0)$.

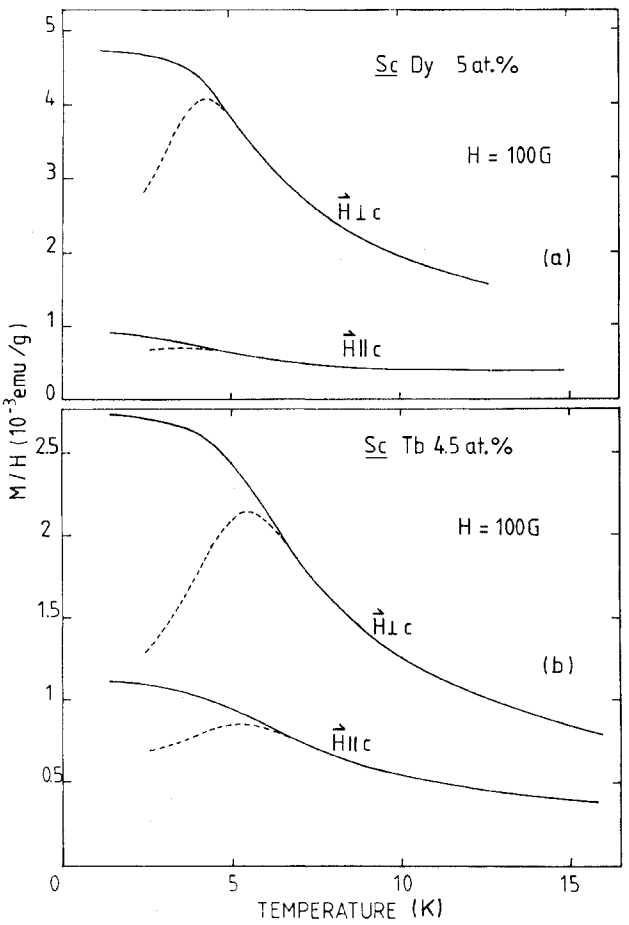

FIG. 4. ZFC (dashed line) and FC (solid line) susceptibilities of (a) ScDy 5 at. % and (b) ScTb 4.5 at. % in transverse and longitudinal fields. In both alloys and for both field directions the temperature of the maximum is lower than the temperature where the ZFC curve departs from the FC one.

and YEr 2 at. %. For *H parallel to the c axis,* both alloys exhibit a sharp cusp of the ZFC susceptibility at a temperature Θ and a splitting of the ZFC and FC curves below Θ. For *H in the basal plane,* the behaviors of YEr and ScEr are different. The transverse susceptibility of YEr 2 at. % does not show any anomaly at the temperature T_g where a cusp is observed in the longitudinal susceptibility. Moreover, the FC and ZFC transverse susceptibility coincide down to the lowest temperature in our experiments. In contrast, the transverse ZFC susceptibility of ScEr 10 at. % exhibits a bifurcation at the *temperature (Θ) of the cusp of the longitudinal susceptibility* and the ZFC curve departs from the FC curve below this temperature.

We have found for all our YEr alloys the same behavior as that of YEr 2 at. %. Since D/j is large for all these YEr alloys (see Table II), their experimental behavior is in agreement with the top of Fig. 1, i.e., with a freezing of only the longitudinal spin components. D/j is definitely smaller for ScEr 10 at. % (see Table II), so that the existence of freezing in both longitudinal and transverse directions is not surprising. However, our results suggest that the freezing temperature is the same for both directions.

We show the field dependence of Θ for YEr 2 at. % in the inset of Fig. 3. The experimental points are approximately on an Almeida-Thouless—like line corresponding to $H^{2/3}\sim 1-\Theta/T_g$.[12,13] However, a fit with the theoretical expression of the Almeida-Thouless (AT) line is only obtained with $g_{\text{eff}}=3.3$ for the doublet ground state instead of $g_{\text{eff}}=14.4$ for the ground state of Table II.[14] This discrepancy of a factor of 4 is surprising in view of the good agreement for YEr 4 at. %.[6] However, one should recall that the theory assumes a Gaussian distribution $P(J_{ij})$ and deviations from such a distribution change the scaling. Significant deviations from a Gaussian distribution are likely to exist in YEr 4 at. % because, for 4 at. % impurities in an hcp lattice, the probabilities of having one nearest neighbor (out of 12) or one of the many (32) next-nearest neighbor lattice sites occupied by an impurity are almost equal.

B. ScDy, ScTb, YDy, and YTb (X-Y—like alloys)

We show the FC and ZFC susceptibilities of YDy 3 at. %, YTb 1 at. %, ScDy 5 at. %, and ScTb 4.5 at. % alloys in Figs. 4—6. As for the alloys with Er impurities, there is a different behavior for the Y-based alloys, for which $|D|/j$ is large, and the Sc-based alloys, for which

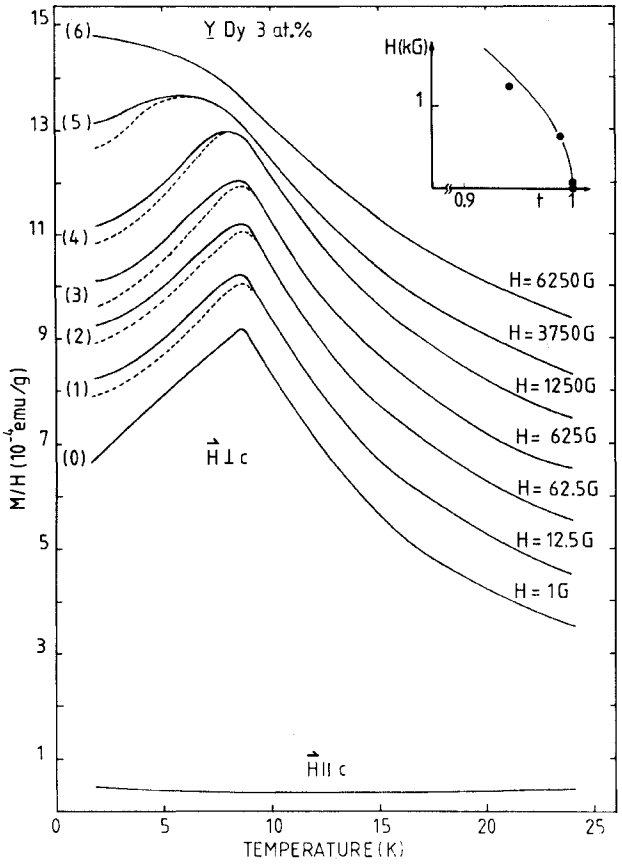

FIG. 5. ZFC (dashed line) and FC (solid line) susceptibilities of YDy 3 at.%. Inset: Field H vs $t=\Theta/T_g$, where Θ is defined as the temperature where the ZFC curve departs from the FC one. The full line corresponds to $H^2 \sim 1-t$.

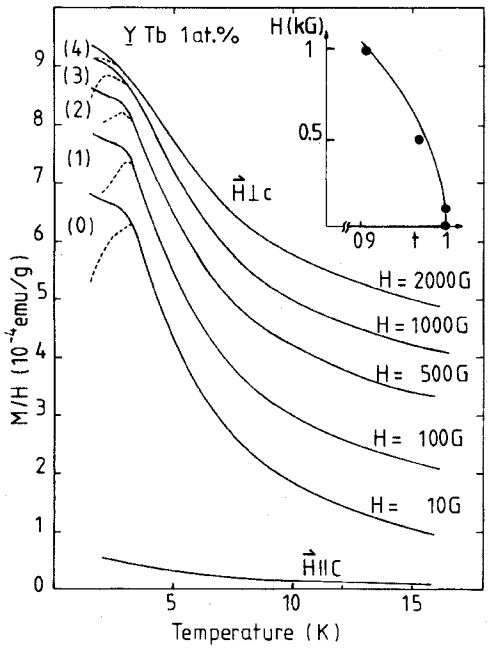

FIG. 6. As Fig. 5 but for YTb 1 at.%.

$|D|/j$ is small.

In the Y-based alloys a maximum of the ZFC susceptibility and a splitting of the FC and ZFC curves at low temperature is observed only in transverse fields. In longitudinal field there is no susceptibility maximum, and the FC and ZFC curves coincide down to the lowest experimental temperatures.

In the Sc-based alloys a maximum of the ZFC susceptibility and a splitting between the FC and ZFC susceptibilities is observed in both longitudinal and transverse fields. Again the temperature (Θ) of the splitting between the FC and ZFC curves is the same (within the experimental error) in longitudinal and transverse fields. The temperature (Θ') of the maximum of the ZFC susceptibility is also the same in longitudinal and transverse fields but is different from Θ.

A general feature observed for all our X-Y—like alloys is that the temperature Θ of the splitting between the FC and ZFC susceptibilities is always higher than the temperature Θ' of the maximum of the ZFC susceptibility (Figs. 4—6). This behavior resembles what is predicted for Heisenberg spin-glasses on the basis of the SK Hamiltonian, that is, a splitting between the FC and ZFC curves at the Gabay-Toulouse (GT) temperature,[13] corresponding to the applied field and a maximum of the ZFC curves near the Almeida-Thouless temperature (see Fig. 7). Moreover, we find (see inset of Figs. 5 and 6) that the field dependence of Θ corresponds approximately to $1-\Theta/T_g \sim H^2$, in agreement with what is expected for the GT line. Thus it appears that our X-Y—like systems follow the behavior predicted for $m \geq 2$. In contrast, our ScEr and YEr follow the behavior expected for Ising spin-glasses (see Fig. 7), with a splitting between the FC and the ZFC curves, a maximum of the ZFC curve at the same Θ, and $1-\Theta/T_g \sim H^{2/3}$. However, it is difficult to understand why the behavior predicted for Heisenberg spin-glasses should be observed in X-Y spin-glasses and not in ScGd or in the classical Heisenberg spin-glasses such as CuMn, AgMn, etc.

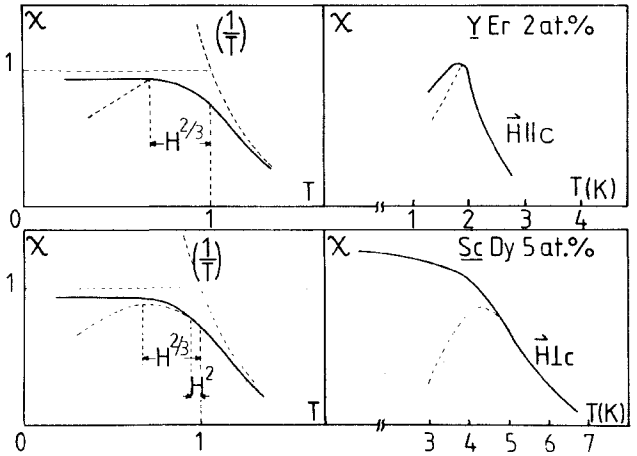

FIG. 7. Schematic difference between the susceptibility of the Ising and Heisenberg infinite-range models around T_g [from Sherrington (Ref. 16)]. Experimental examples for Ising-like (Er) and X-Y—like (Dy) systems are shown on the right-hand side.

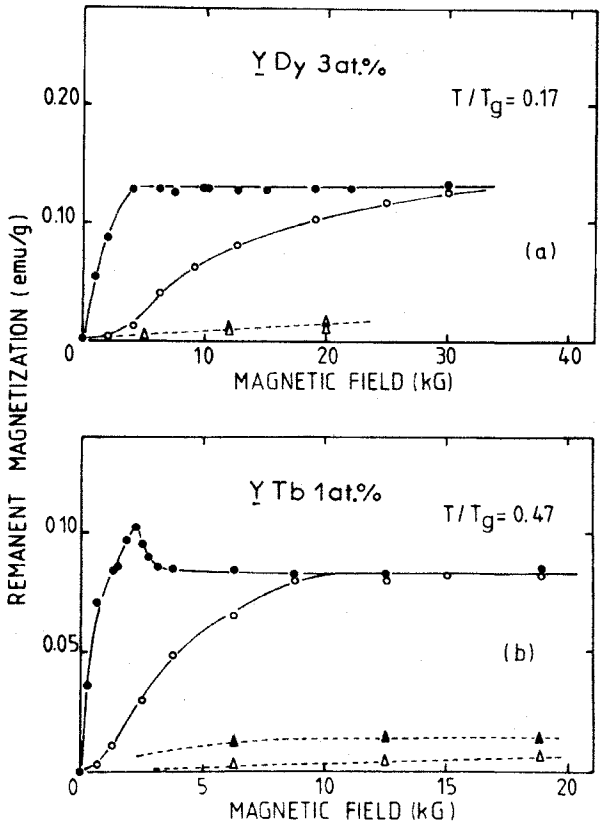

FIG. 8. TRM (closed symbols) and IRM (open symbols) for (a) YDy 3 at.% and (b) YTb 1 at.% in transverse (circles) or longitudinal (triangles) fields.

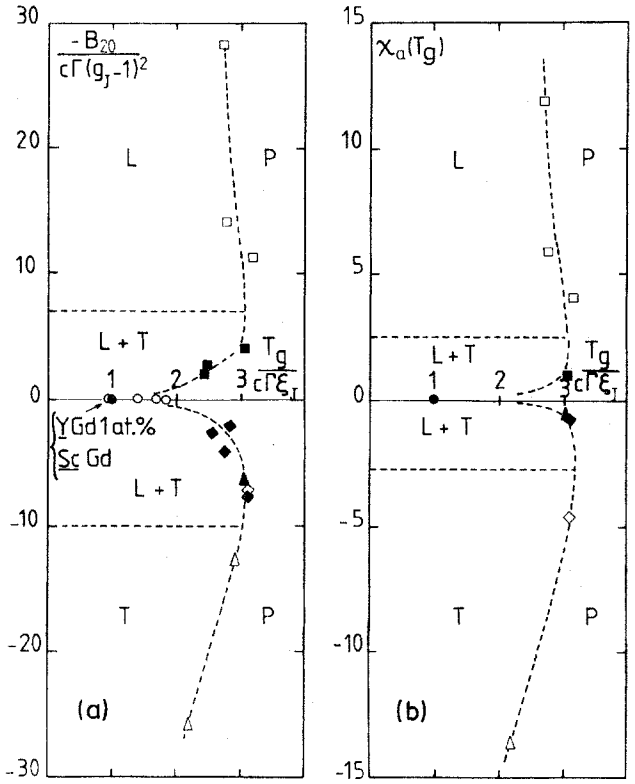

FIG. 9. Experimental phase diagram for the Sc- and Y-based alloys (to be compared to the theoretical phase diagram of Fig. 1). (a): $-B_2^0/[c\Gamma(g_J-1)^2]\equiv D/j$ vs $T_g/(c\Gamma\xi_J)\equiv T_g/j$ (see Sec. II for the notation). (b): Experimental anisotropy-exchange ratio [see Eq. (11)] vs $T_g/(c\Gamma\xi_J)\equiv T_g/j$. The experimental data correspond to YEr (□), ScEr (■), YDy (◇), ScDy (◆), YTb (△), ScTb (▲), YGd (○) and ScGd (●) alloys. The number of experimental points is smaller in (b) because $\chi_a(T_g)$ is known only for single crystals.

We have also studied the remanence properties of some Y- and Sc-based alloys. The results on YEr have already been presented in Refs. 4 and 6. We show in Fig. 8 the TRM and IRM of YDy and YTb alloys for H in the basal plane. The variation of the TRM and the IRM as a function of H is that usually observed in spin-glasses. For H parallel to the c axis the remanences of these two alloys are vanishingly small.

C. *Sc*Gd and *Y*Gd (Heisenberg-like alloys)

The *Sc*Gd system exhibits typical spin-glass properties: a sharp cusp of the ZFC susceptibility in low fields, strong broadening of the cusp in moderate fields, and splitting of the FC and ZFC susceptibility curves below the temperature of the cusp. Its susceptibility is nearly, but not completely, isotropic.

The *Y*Gd system appears to be a more complex disordered magnetic system because it exhibits a sharp cusp but does not show irreversibility properties below the temperature of the cusp. Its magnetic behavior is also weakly anisotropic.

We plan to report on the magnetic properties of *Sc*Gd and *Y*Gd and discuss the origin of their weak anisotropy in a future publication.[17] In this paper we will only compare their freezing temperature with that of the other Sc- and Y-based alloys (next section).

D. Phase diagram

In Fig. 9(a) we plot the values of D/j vs T_g for all our Sc- and Y-based alloys. The values of D/j are calculated as explained in Sec. II. We choose T_g as the low-field limit of the temperature at which the FC susceptibility curve departs from the ZFC curve in Figs. 2–6. We have plotted the values of D/j and T_g of polycrystalline samples as well as those for the single-crystal alloys studied in the present work. All the values of D/j and T_g are listed in Table II. By comparing Fig. 9(a) with the theoretical phase diagram of Fig. 1, one is led to the following conclusions.

(i) The most remarkable agreement of Fig. 9(a) with Fig. 1 is for the ratio of about 3 between the values of T_g/j in the Ising and Heisenberg limits, $D/j\gg 1$ and $D/j=0$, respectively. In contrast, the ratio between the experimental values of T_g/j in the X-Y and Heisenberg limits is definitely larger than the value 1.5 predicted by theory.

(ii) As D/j varies from large and positive values to large and negative values, the experimental variation of T_g, with a depression of T_g around $D/j=0$, is qualita-

tively the same as that predicted by theory and represented in Fig. 1. A small difference is the existence of a maximum of T_g, i.e., the bulge at intermediate values of $|D/j|$.

(iii) At large values of $|D/j|$ [open symbols in Fig. 9(a)] irreversibility effects are observed only for longitudinal (or transverse) fields. At small values of $|D/j|$ [full symbols in Fig. 9(a)] irreversibilities are observed in *both directions* below the *same temperature* and our experiments are unable to identify a second transition line at a lower temperature, i.e., the transitions L→LT or T→LT in Fig. 1. However, since the theoretical papers Refs. 1 and 2 predicting the second transition do not describe how it can be detected, we cannot completely rule out its existence.

In the above discussion of the properties of the Sc- and Y-based alloys as a function of the parameter $D/j \sim B_2^0/c$, we have neglected the existence of higher-order crystal-field terms. However, these terms are not completely negligible (see Table I); for example, the term $B_6^6 O_6^6$ mixes $|J,M\rangle$ and $|J,M\pm 6\rangle$ states and reduces the anisotropy of the spin system. When such effects are significant, the ratio $D/j \sim B_2^0/c$ is no longer the characteristic parameter of the anisotropy, and it may be better to characterize the anisotropy exchange ratio by the experimental parameter

$$\chi_a(T_g)=\frac{3}{c}\left[\frac{X_{\parallel}-X_{\perp}}{X_{\parallel}+2X_{\perp}}\right]\Bigg|_{T=T_g}. \tag{11}$$

In Fig. 9(b) we have plotted on the vertical axis the values of $\chi_a(T_g)$ instead of those of D/j. The graph obtained in this way is not very different from that of Fig. 9(a), and we are led to the same conclusions. Note that $\chi_a(T_g)$ cannot be derived for polycrystalline samples, so only the results on single crystals appear in Fig. 9(b).

E. Mixed alloys: *Sc*ErDy and *Y*ErDy

In Fig. 10(a) we show the FC and ZFC susceptibility curves of a single crystal of Y containing 2.2 at. % of ER and 2 at % of Dy. The experimental behavior is that of two spin systems which are almost decoupled: The transverse susceptibility presents a cusp at 5 K and is approximately that of an alloy *Y* Dy 2 at. % for which T_g is expected to be about 6 K. There is no anomaly at 5 K in longitudinal fields. The longitudinal susceptibility shows a cusp at about 1.6 K [see inset of Fig. 10(a)] and is approximately that of an alloy *Y* Er 2.2 at. % for which T_g is expected to be about 2 K.

Figure 10(b) shows the susceptibility of a polycrystalline sample of Sc containing 12 at. % Er and 3 at. % Dy. The freezing temperatures of *Sc*Er 12 at. % and *Sc*Dy 3 at. % would be 3.5 and 2.7 K, respectively. The susceptibility of the ternary alloy exhibits a unique cusp at $T_g \simeq 6$ K, which is approximately the sum of 3.5 and 2.7 K. This additivity implies a coupling of the Er and Dy spin systems.

Viana and Bray[15] have extended their earlier model[2] to the case of spin-glasses with mixed uniaxial anisotropies. They predict different freezing temperatures for the longitudinal and transverse components in alloys such as ours. The experimental results on *Y* ErDy are consistent with this prediction and, more generally, with the idea that in the limit of strong anisotropies spins with only longitudinal components and spins with only transverse components cannot be coupled by isotropic exchange. On the other hand, our results on *Sc*ErDy suggest a unique freez-

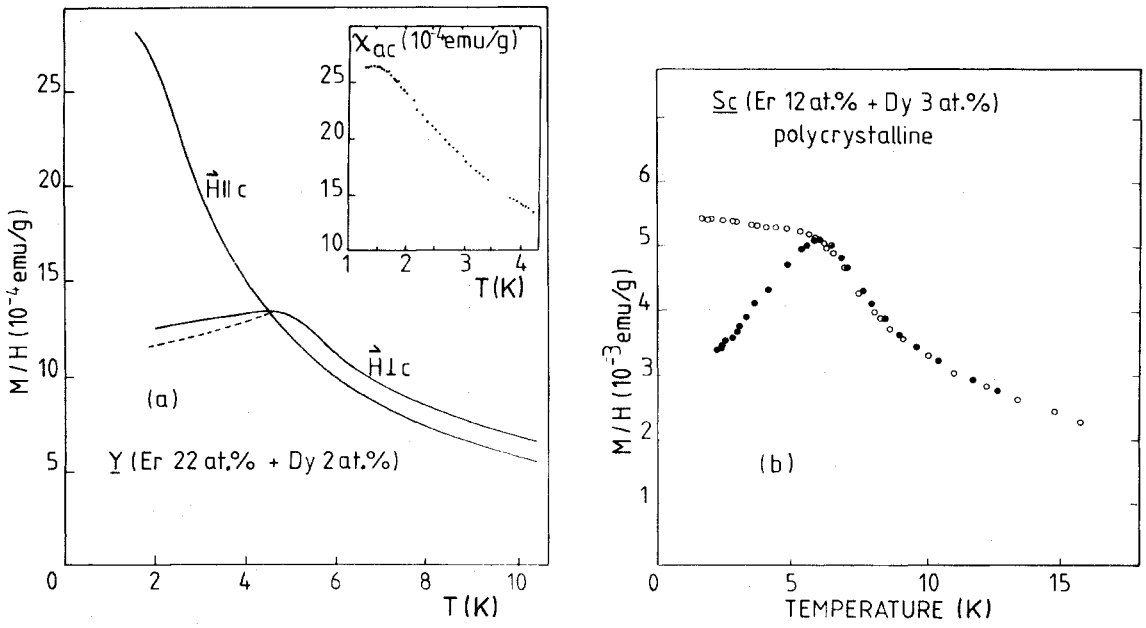

FIG. 10. FC [solid lines in (a) and open circles in (b)] and ZFC [dashed lines in (a) and full circles in (b)] susceptibilities (a) for a single crystal of Y with 2.2 at. % of Er and 2 at. % of Dy and (b) for a polycrystal of Sc with 12 at. % of Er and 3 at. % of Dy. Inset: ac susceptibility of the sample of *Sc*ErDy in longitudinal fields.

ing temperature in this alloy; this disagrees with the predictions of Viana and Bray. However, independent measurements of the longitudinal and transverse susceptibilities in a single crystal of *Sc*ErDy would be of interest to confirm that there is a unique freezing temperature.

IV. CONCLUSIONS

We have investigated the magnetic properties of single crystals of Sc and Y containing rare-earth impurities and have compared our results with the predictions of the models of Sherrington and Cragg[1] and Roberts and Bray[2] for uniaxial spin-glasses.

An interesting result is the resemblance of the theoretical (see Fig. 1) and experimental (see Fig. 9) phase diagrams. There is a remarkable agreement of our results with theory for the ratio 3 between the values of T_g/j in the Ising and Heisenberg limits. On the other hand, the agreement with theory is only qualitative when one compares the values of T_g/j in X-Y and Heisenberg limits. We point out that the dependence of T_g/j on spin dimension seems to appear also in the *Zn*Mn (Ising-like, $T_g/c \cong 22$ K/at.%), *Cd*Mn (X-Y—like, $T_g/c \cong 11$ K/at.%), and *Mg*Mn (Heisenberg-like, $T_g/c \cong 3$ K/at.%) spin-glasses.[3] However, a quantitative comparison is questionable for these spin-glasses with different host metals.

Another striking result is the difference between the susceptibility-versus-temperature curves of the Ising-like and X-Y—like alloys. In the Ising-like alloys, at the temperature Θ where the ZFC curve departs from the FC, one finds the maximum of the ZFC susceptibility, and Θ depends approximately on the applied field according to $H^{2/3} \sim 1 - \Theta/T_g$. This is what is expected for Ising SK spin-glasses.[16] In contrast, in the X-Y—like alloys, Θ is higher than the temperature of the maximum of the ZFC susceptibility and depends approximately on H according to $H^2 \sim 1 - \Theta/T_g$. When Θ is identified as the Gabay-Toulouse temperature, this is what is expected for $m \geq 2$ spin-glasses (see Fig. 7 and Ref. 16). If this interpretation is correct, it would be the first experimental identification of the GT line. However, it remains to explain why this behavior is found in our X-Y systems and not in classical Heisenberg spin-glasses such as *Cu*Mn.

The last question to answer is the following: Are the $Y\mathscr{R}$ alloys (where $\mathscr{R}$ represents a rare-earth element) good spin-glasses in spite of their tendency to form a helical or modulated magnetic structure? According to Sarkissian and Coles[18] the $Y\mathscr{R}$ alloys are spin-glasses at low concentrations (in our concentration range) and develop long-range order above 4 or 5 at.%. However some recent experiments have found characteristic properties of some sort of long-range order in YGd, down to 1 at.%.[19] Although we cannot completely rule out a trace of long-range order in our YEr, YDy, YTb alloys, our basic assumption in this paper has been to neglect such effects and to consider our Y-based alloys as "uniaxial spin-glasses." Note that the Sc-based alloys are much less suspect to develop some long-range order: *Sc*Gd, in contrast to *Y*Gd, exhibits very classical spin-glass properties and, according to Sarkissian and Coles,[18] helical ordering appears only above approximately 23 at.% in *Sc*Gd or *Sc*Tb.

ACKNOWLEDGMENTS

We thank H. Bouchiat, I. A. Campbell, M. Gabay, P. Monod, and P. Touborg for many helpful discussions. We thank P. Touborg for providing us with one of the samples. We thank W. Wisny, Freie Universität Berlin (FUB) for performing some of the measurements and C. Kähler (FUB) for growing some of the single crystals. One of us (K.B.) would like to thank the Laboratoire de Physique des Solides for its hospitality during his stay at Orsay. This work was supported in part by Deutsche Forschungsgemeinschaft, Sonderforschungsbereich 161.

*Permament address: Institute für Atom und Festkörperphysik, Freie Universität Berlin, Arnimallee 14, D-1000 Berlin 33, West Germany.

[1]D. M. Cragg and D. Sherrington, Phys. Rev. Lett. 49, 1120 (1982); D. Sherrington, D. M. Cragg, and D. J. Elderfield, J. Magn. Magn. Mater. 31-34, 1417 (1983).

[2]S. A. Roberts and A. J. Bray, J. Phys. C 15, L 527 (1982); A. J. Bray and L. Viana (unpublished).

[3]H. Albrecht, E. F. Wassermann, F. T. Hedgcock, and P. Monod, Phys. Rev. Lett. 48, 819 (1982).

[4]A. Fert, P. Pureur, F. Hippert, K. Baberschke, and F. Bruss, Phys. Rev. B 26, 5300 (1982).

[5]K. D. Usadel, K. Bien, and H. J. Sommers, Phys. Rev. B 27, 6957 (1983).

[6]R. Wendler and K. Baberschke, Solid State Commun. 48, 91 (1983).

[7]D. Sherrington and S. Kirkpatrick, Phys. Rev. Lett. 35, 1972 (1975).

[8]J.R.L. de Almeida, R. C. Jones, J. M. Kosterlitz, and D. J. Thouless, J. Phys. C 11, L871 (1978).

[9]P. Touborg, Phys. Rev. B 16, 1201 (1977); Ph.D. thesis, Universität Darmstadt, 1978 (unpublished).

[10]G. Keller and J. M. Dixon, J. Phys. F 6, 819 (1976); G. Keller, Ph.D. thesis, Universität Odense, 1975 (unpublished).

[11]A. Abragam and B. Bleaney, *Electron Paramagnetic Resonance of Transition Ions* (Oxford University Press, New York, 1970).

[12]A careful study of the AT line of YEr has been done independently by H. Bouchiat and P. Monod (unpublished).

[13]J.R.L. de Almeida and D. J. Thouless, J. Phys. A 11, 983 91978); M. Gabay and G. Toulouse, Phys. Rev. Lett. 47, 201 (1981).

[14]There is a principle ambiguity in adapting the classical spin s (from theory) to the quantum-mechanical operator $\vec{J}$ or $\vec{S}$. Whether one adjusts for equal Zeeman splitting or equal susceptibility the prefactor of h changes.

[15]L. Viana and A. J. Bray (unpublished).

[16]D. Sherrington, in *Heidelberg Colloquium on Spin Glasses,* Vol. 192 of *Lecture Notes in Physics,* edited by J. L. van Hemmen and I. Morgenstern, (Springer, New York, 1983, p. 125.

[17]R. Wendler, P. Pureur, A. Fert, and K. Baberschke, J. Magn. Magn. Mater. (in press).

[18]B.V.B. Sarkissian and B. R. Coles, Commun. Phys. 1, 17 (1976).

[19]L. E. Wenger and J. A. Mydosh, J. Appl. Phys. (in press).